PERGAMON

Chemical Engineering Science 56 (2001) 1869–1881

Chemical Engineering Science

www.elsevier.nl/locate/ces

Reaction-transport simulations of non-oxidative methane conversion with continuous hydrogen removal — homogeneous–heterogeneous reaction pathways

Lin Li[a,b], Richard W. Borry[a,b], Enrique Iglesia[a,b,*]

[a]*Department of Chemical Engineering, University of California at Berkeley, 201, Gilman Hall #1462, Berkeley, CA 94720, USA*
[b]*Division of Materials Sciences, E.O. Lawrence Berkeley National Laboratory, University of California at Berkeley, 201, Gilman Hall #1462, Berkeley, CA 94720, USA*

Received 9 March 2000; received in revised form 11 August 2000; accepted 20 August 2000

Abstract

Detailed kinetic-transport models were used to explore thermodynamic and kinetic barriers in the non-oxidative conversion of CH_4 via homogeneous and homogeneous–heterogeneous pathways and the effects of continuous hydrogen removal and of catalytic sites on attainable yields of useful C_2–C_{10} products. The homogeneous kinetic model combines separately developed models for low-conversion pyrolysis and for chain growth to form large aromatics and carbon. The H_2 formed in the reaction decreases CH_4 pyrolysis rates and equilibrium conversions and it favors the formation of lighter products. The removal of H_2 along tubular reactors with permeable walls increases reaction rates and equilibrium CH_4 conversions. C_2–C_{10} yields reach values greater than 90% at intermediate values of dimensionless transport rates ($\delta = 1$–10), defined as the ratio hydrogen transport and methane conversion rates. Homogeneous reactions require impractical residence times, even with H_2 removal, because of slow initiation and chain transfer rates. The introduction of heterogeneous chain initiation pathways using surface sites that form methyl radicals eliminates the induction period without influencing the homogeneous product distribution. Methane conversion, however, occurs predominately in the chain transfer regime, within which individual transfer steps and the formation of C_2 intermediates become limited by thermodynamic constraints. Catalytic sites alone cannot overcome these constraints. Catalytic membrane reactors with continuous H_2 removal remove these thermodynamic obstacles and decrease the required residence time. Reaction rates become limited by homogeneous reactions of C_2 products to form C_{6+} aromatics. Higher δ values lead to subsequent conversion of the desired C_2–C_{10} products to larger polynuclear aromatics. We conclude that catalytic methane pyrolysis at the low temperatures required for restricted chain growth and the elimination of thermodynamics constraints via continuous hydrogen removal provide a practical path for the direct conversion of methane to higher hydrocarbons. The rigorous design criteria developed are being implemented using shape-selective bifunctional pyrolysis catalysts and perovskite membrane films in a parallel experimental effort.

Keywords: Methane; Pyrolysis; Kinetics; Simulation; Reaction Engineering; Membranes

1. Introduction

The direct conversion of methane to fuels and petrochemicals remains a formidable challenge. Oxidative coupling on metal oxides (Keller & Bhasin, 1982; Ito & Lunsford, 1985; Tonkovich, Car, & Aris, 1993; Jiang, Yentekakis, & Vayenas, 1994) and non-oxidative reactions on Mo/H-ZSM5. (Wang, Tao, Xie, & Xu, 1993; Solymosi, Erdohelyi, & Szoka, 1995; Solymosi, Cserenyi, Szoke, Bansagi, & Oszko, 1997; Wang, Lunsford, & Rosynek, 1996) to form C_{2+} hydrocarbons remain the most promising approaches. C_{2+} yields in oxidative coupling reactions using co-feed or cyclic redox reactors are limited to about 25%, because the required O_2 co-reactant reacts unselectively to form CO and CO_2 via homogeneous and surface-catalyzed pathways. Unfavorable thermodynamics limit hydrocarbon yields in non-oxidative methane conversion reactions ($\sim$12% benzene at 973 K and 1 bar CH_4) (Lunsford, Rosynek, & Wang, 1995). Thermodynamic estimates show that high temperatures and low H_2 concentrations increase

* Corresponding author. Tel.: +1-510-642-9673; fax: +1-510-642-4778.
E-mail address: iglesia@cchem.berkeley.edu (E. Iglesia).

0009-2509/01/$ - see front matter
PII: S0009-2509(00)00465-6

hydrocarbon yields, but they also lead to increasingly unsaturated products and to the preferential formation of polynuclear aromatics and carbon (Gueret, Daraux, & Brilland, 1997). At lower temperatures (<1473 K), homogeneous pyrolysis reactions are slow, but they form ethylene and benzene with modest selectivity. The presence of added H_2 decreases homogeneous reaction rates and the methane conversion level attainable at equilibrium. Thus, the removal of H_2 during pyrolysis reactions may benefit homogeneous reaction pathways and lead to practical reaction rates. H_2 also decreases the selectivity to polynuclear aromatics and increases the hydrogen content within pyrolysis products (Rokstad, Olsvik, Jessen, & Holmen, 1992; Gueret et al., 1997). The kinetics effects of H_2 concentration, and thus of hydrogen removal rates, are complex; selectivity and rate effects are intertwined within complex homogeneous pathways, which must be described in detail in order to design optimum practical processes.

Several groups have used hydrogen-selective transport membranes in attempts to couple non-oxidative methane conversion with H_2 oxidation and to eliminate thermodynamic constraints in CH_4 pyrolysis and the high CO_x yields in oxidative coupling (Andersen et al., 1989; Woldman & Sokolovskii, 1991; Hamakawa, Hibino, & Iwahara, 1993, 1994; Langguth et al., 1997). As a side benefit, such an approach avoids the need for O_2 separation from air, a step required in co-feed oxidative coupling reactors in order to prevent dilution by N_2. Scheme 1 shows a schematic diagram for methane conversion in a catalytic membrane reactor. CH_4 and air flow on the two opposite sides of a hydrogen-selective membrane. CH_4 reacts via pyrolysis pathways to form C_{2+} hydrocarbons on one side; hydrogen migrates across the membrane, and all or part of it reacts with the O_2 in air to form water. The latter reaction provides the enthalpy and free energy required for the overall reaction and it establishes the chemical potential gradient required for hydrogen transport across the membrane. Previous attempted implementations of this concept have led to disappointing results, in spite of qualitative theoretical support. Hydrogen transport membranes based on Pd or Pd/Ag alloys led to rapid carbon deposition on one side and to membrane oxidation on the opposite side (Andersen et al., 1989). Above 1100 K, $SrCe_{0.95}Yb_{0.05}O_3$ proton-conductors, which avoid these structural changes, become oxygen conductors and form CO_x on the CH_4 side (Langguth, Dittmeyer, Hofmann, & Tomandl, 1997) Hamakawa et al. reported 100% C_2 selectivity using $SrCe_{0.95}Yb_{0.05}O_{3-\alpha}$ ceramic membranes at 900°C, but methane conversions were very low (<1%) because of the absence of an effective catalyst for methane pyrolysis reactions. The higher reaction temperatures required in order to increase reaction rates led to extensive carbon deposition on the Ag electrode and on the membrane (Hamakawa et al., 1993, 1994).

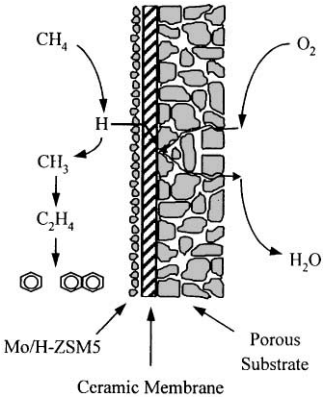

Scheme 1.

In addition to the challenges imposed by the synthesis and operation of the required ceramic membranes, the removal of hydrogen during methane pyrolysis poses design and optimization issues that can be addressed most effectively by rigorous simulations of homogeneous and coupled homogeneous–heterogeneous methane pyrolysis pathways. These issues include the contrasting kinetic effects of H_2 on the pyrolysis rate and selectivity, the maximum yields of C_2–C_{10} hydrocarbons attainable in membrane reactors, and the balance between CH_4 conversion and H_2 removal rates required to achieve these maximum C_2–C_{10} yields.

Here, we use a detailed kinetic-transport model in order to simulate homogeneous pyrolysis reactions of methane in a membrane reactor. The model includes a kinetic network that extends previous proposals accurate only at low conversions (Dean, 1990) by incorporating a kinetic lumping approach that describes chain growth pathways (Wang & Frenklach, 1997) prevalent at the higher conversions feasible when H_2 is continuously removed. In addition, the nature of the rate-determining steps in homogeneous pyrolysis sequences is examined in order to suggest specific catalytic steps required in order to overcome the significant kinetic barriers inherent in purely homogeneous pyrolysis pathways.

2. Kinetic-transport models and simulation methods

2.1. Kinetic model of homogeneous methane pyrolysis

A reduced homogeneous methane pyrolysis kinetic model consisting of 44 elementary steps and 25 species (Dean, 1990) was used as one component of our kinetic network. At low CH_4 conversions (<1%), this model accurately describes homogenous methane conversion data at 1038 K and 59 kPa CH_4 (Dean, 1990). As methane conversion increases, however, the formation of

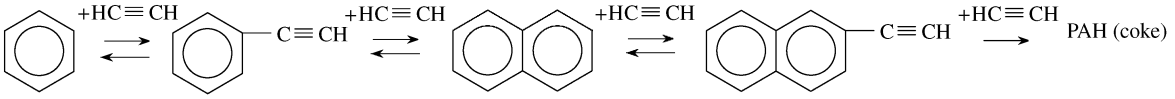

Scheme 2. The growth of polyaromatic hydrocarbon.

high-molecular weight aromatics and solid carbon becomes important and this kinetic model must be modified in order to account for the higher conversions attainable, even at low temperatures, as H_2 is continuously removed during methane reactions. We consider in our simulations all species larger than naphthalene ($C_{10}H_8$) as undesired polynuclear aromatic hydrocarbons (PAH). We monitor the concentration of these species as a lump, but describe the kinetics of their formation from benzene and naphthalene, rigorously and without lumping approximations, as a function of reactor residence and of H_2 concentration. We assume that the growth of polyaromatic hydrocarbons occurs predominately via a H-abstraction/C_2H_2-addition mechanism (Wang & Frenklach, 1997). As shown in Scheme 2, eight elementary steps were introduced into the pathways previously proposed (Dean, 1990) in order to describe methane pyrolysis at low temperatures and high methane conversion and to account for the formation of hydrocarbons larger than naphthalene during homogeneous methane pyrolysis with continuous hydrogen removal (see Table 1 for the eight steps added). The rate constants and the thermodynamic data for these steps were obtained from previous reports (Wang & Frenklach, 1997).

With the addition of these steps describing PAH formation, the complete homogeneous methane pyrolysis kinetic model consists of 52 elementary steps involving the reactions of 33 species. Table 1 lists additional modifications introduced into the pyrolysis mechanism of Dean (1990) as a result of recent thermodynamic data for several radicals, which influence the estimates for reverse rate constants for any steps involving these radicals. Only reactions with rate constants differing by more than 5% from those in the original Dean kinetic network are included in Table 1. The parameters used to estimate forward rate constants can be found in the original reference (Dean, 1990).

Catalytic sites can activate C–H bonds in CH_4 to form methyl radicals and hydrogen. The methyl radicals can then desorb and increase the rate of homogeneous pyrolysis pathways. Such catalytic sites are incorporated into our simulations by introducing the following elementary step:

$$CH_4 + [*] \overset{k_{s1}}{\rightarrow} CH_3\cdot + [^*H] \tag{1}$$

in order to examine the effect of catalytic activation of CH_4 on the overall rate of CH_4 conversion.

2.2. Simulations of hydrogen removal rate

Simulations of the effect of continuous H_2 removal on homogeneous methane pyrolysis rate and selectivity require an equation that relates the rate of H_2 removal to the H_2 concentration prevalent at any point in a reactor. Diffusive processes are rigorously described by Fick's diffusion equation. The solution to this equation in the slab geometry characteristic of a membrane wall much thinner than the diameter of a tubular reactor is given by

$$J_{H_2} = \frac{P}{l}(p_{H_2,1} - p_{H_2,2}) \tag{2}$$

irrespective of the detailed mechanism of transport. In this equation, P is the permeability of H_2 through the membrane, l is membrane thickness, and $p_{H_2,1}$ and $p_{H_2,2}$ are the hydrogen partial pressure on the feed (CH_4) and permeate (air) sides of the membrane, respectively. Deviations from this equation may occur for certain membrane systems. In such case, the appreciate permeation equation should be used instead of Eq. (2), but the trends and concepts described here will remain largely unaffected by this modification.

2.3. Membrane reactor equations

For a complex reaction system with n reactions involving m components, the reaction rate for component j can be expressed as

$$R_j = \sum_{i=1}^{n} \lambda_{ij} k_i(T,p) f_i(K,p). \tag{3}$$

When these reactions occur in a plug-flow tubular reactor with a permselective wall, a differential mole balance gives the following dimensionless differential equations:

$$\frac{1}{Da}\frac{d\phi_j}{d\xi} = \sum_{i=1}^{n} \lambda_{ij}\beta_i f_i(K,p) - \delta\alpha_j(y_{jt} - y_{js}), \tag{4}$$

$$\frac{1}{Da}\frac{dq_j}{d\xi} = \delta\alpha_j(y_{jt} - y_{js}), \tag{5}$$

where

$$Da = Lk_1/F_{10} = \text{Damkohler number} = \frac{\text{reactant conversion rate}}{\text{reactant inlet molar rate}}, \tag{6}$$

Table 1
Additions and changes to the Dean CH_4 pyrolysis mechanism Dean (1990) (1038 K, 0.59 bar)

Reaction[a]	k_f[b]	k_r	Reference
$C=CC=C=CC\cdot + H$	3.74E − 04	6.17E + 13	
$C=CC=C_2H_3 + CH_3$	7.54E − 04	1.53E + 14	Dean (1990)
$CY13PD = CY13PD5\cdot + H$	2.24E − 01	4.44E + 14	Dean (1990)
$CH_3 + CY13PD5\cdot = CHD$	2.39E + 12	8.60E + 01	Dean (1990)
$CH_3 + CY13PD5\cdot = CYC_6H_7 + H$	1.06E + 09	2.72E + 13	Dean (1990)
$2CY13PD5\cdot = NAPH + H_2$	1.29E + 08	9.73E − 06	Dean (1990)
$C_2H_3 = C_2H_2 + H$	1.24E + 03	7.98E + 10	Dean (1990)
$CYPENE4\cdot = C=CCC=C\cdot$	1.05E + 06	3.87E + 09	Dean (1990)
$CYPENE4\cdot = CY13PD + H$	8.56E + 05	1.07E + 12	Dean (1990)
$CY13PD + H = H_2 + CY13PD5\cdot$	9.34E + 12	7.82E + 06	Dean (1990)
$C_2H_4 + CH_3 = C_2H_3 + CH_4$	1.93E + 09	1.08E + 10	Dean (1990)
$CY13PD + CH_3 = CH_4 + CY13PD5\cdot$	2.16E + 10	3.77E + 05	Dean (1990)
$H + C=CC=CCC\cdot$	1.45E + 12	1.42E + 05	Dean (1990)
$H + C\#CC=CC=C\cdot$	6.65E + 11	8.24E + 04	Dean (1990)
$CH_3 + C_2H_4 = CCC\cdot$	6.78E + 09	2.09E + 06	Dean (1990)
$CH_3 + C_2H_2 = CC=C\cdot$	1.34E + 10	2.38E + 06	
$CH_3 + C=CC=C=CCC + H$	3.70E + 07	8.06E + 11	Dean (1990)
$CH_3 + C=C=C=C_2H_3 + C_2H_4$	1.34E + 08	8.98E + 07	Dean (1990)
$C=CC\cdot + C_2H_2 = C=CCC=C\cdot$	2.49E + 09	2.24E + 08	Dean (1990)
$C=CC\cdot + C_2H_2 = CYPENE4\cdot$	7.30E + 09	1.79E + 05	Dean (1990)
$C=CC\cdot + C_2H_2 = CY13PD + H$	2.95E + 09	9.00E + 10	Dean (1990)
$C=CC\cdot + CY13PD5\cdot = C=C=C + CY13PD$	1.00E + 12	2.08E + 08	Dean (1990)
$C_6H_6 + H = C_6H_5\cdot + H_2$	1.07E + 11	4.81E + 10	Wang and Frenklach (1997)
$C_6H_5\cdot + C_2H_2 = C_6H_5C_2H + H$	9.05E + 10	6.40E + 11	Wang and Frenklach (1997)
$C_6H_5C_2H + H = C_6H_4\cdot C_2H + H$	1.07E + 11	2.74E + 11	Wang and Frenklach (1997)
$C_6H_4\cdot C_2H + C_2H_2 = NAPH\cdot$	1.43E + 11	8.27E − 04	Wang and Frenklach (1997)
$NAPH + H = NAPH\cdot + H_2$	1.07E + 11	1.84E + 11	Wang and Frenklach (1997)
$NAPH\cdot + C_2H_2 = NAPHC_2H + H$	1.34E + 10	5.84E + 10	Wang and Frenklach (1997)
$NAPHC_2H + H = NAPH\cdot C_2H + H_2$	1.07E + 11	4.43E + 11	Wang and Frenklach (1997)
$NAPH\cdot C_2H + C_2H_2 \rightarrow COKE$	1.43E + 11	—	Wang and Frenklach (1997)

[a]Abbreviations: =: double bond; #: triple bond; CY13PD: 1,3-cyclo-pentadiene; CY13PD5·: 1,3-cyclopentadienyl; CHD: 1,3-cyclohexadiene; CYC_6H_7: 1,3-hexadienene; NAPH: naphthalene; CYPENE4·: 4-cyclopentenyl radical.
[b]Unit are s^{-1} (for first order) or $cm^3\,mol^{-1}\,s^{-1}$ (for second order).

$$\delta = \frac{4P_f P_T}{dlk_1} \quad \text{rate ratio} = \text{permeation rate/reaction rate}, \tag{7}$$

$$\alpha_j = P_j/P_f, \tag{8}$$

$$\beta_i = k_i/k_1. \tag{9}$$

The assumptions required in the derivation of these equations are:

(1) isothermal plug flow in both tube and shell sides; no radial concentration or temperature gradients.
(2) Negligible pressure drop on both tube and shell sides.
(3) No boundary layer concentration gradients near the membrane surface.
(4) Membrane permeabilities independent of mixture composition.
(5) H_2 concentrations on the shell side much lower than on the reaction side.

Some of the above assumptions may become invalid for some applications, but they seem reasonable for many designs and they have been customarily made in previous membrane reactor models (Tsotsis, Champagnie, Vasileiadis, & Liu, 1993; Hsieh, 1996). In some applications, radial or axial temperature gradients may exist, pressure drop can be significant at high Reynolds numbers, and the reduction potential of the gas mixture can affect the concentration of various charge carriers and the permeability in ceramic materials.

Several dimensionless parameters (Da, δ, α_i and β_i) arise from the non-dimensionalization of these mole balances. These parameters are defined in terms of a basis reactant, which can be arbitrarily chosen. For example, Da and k_1 can be defined in terms of the forward reaction rate constant for any reaction in the system and F_{10} as the molar inlet flow rate of the basis reactant. Methane, the only reactive molecule in the feed, is chosen here as the basis reactant. This study addresses the consequences of H_2 removal; as a result, it seems reasonable to define

a parameter δ as the ratio of characteristic H_2 transport and CH_4 conversion molar rates. Methane pyrolysis rates, however, are described by a complex kinetic network and the rate constant required to define *Da* and δ cannot be readily obtained from this model by inspection. As a result, we use instead a pseudo-first-order rate constant obtained by fitting simulated reaction rates as a linear function of methane concentration and using parameter estimation to estimate the value of the rate constant giving the best fit. We stress that the simulations are carried out using the complete kinetic model and that this pseudo-first-order rate constant is used merely to examine the nature of the rate-determining steps and to present the results of the simulations in a clearer and more effective manner.

2.4. Computational methods

Simulations were carried out using CHEMKIN II and DVODE subroutines (Kee et al., 1990). Forward rate constants were calculated from modified (three-parameter) Arrhenius equations (Kee, Rupley, & Miller, 1990). Reverse rate constants were obtained from thermodynamic data available for each elementary step. The specific values of the rate constants (except as noted in Table 1) and the sensitivity analysis used to choose the specific elementary steps were reported previously by Dean (1990).

Thermodynamic data were obtained from literature compilations (Stull, Edgar, Westrum, & Sinke, 1987), ab initio calculations (cyclopentadiene and cyclopentadienyl radicals (Karni, Oref, & Burcat, 1991)), or they were estimated using group additivity methods (Benson, 1976; Ritter & Bozzelli, 1991) from parent compounds using hydrogen bond increments for radical species (Lay, Bozzelli, Dean, & Ritter, 1995). CH_4 conversion and product distributions at thermodynamic equilibrium were calculated using STANJAN (Kee & Lutz, 1991), a set of subroutines that minimizes the total Gibbs free energy of complex reacting mixtures.

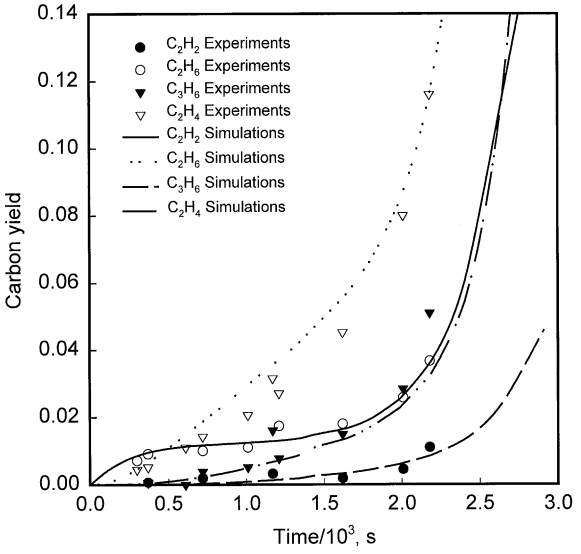

Fig. 1. Homogeneous CH_4 pyrolysis: comparison of simulations vs. experimental results (1038 K, 0.59 bar).

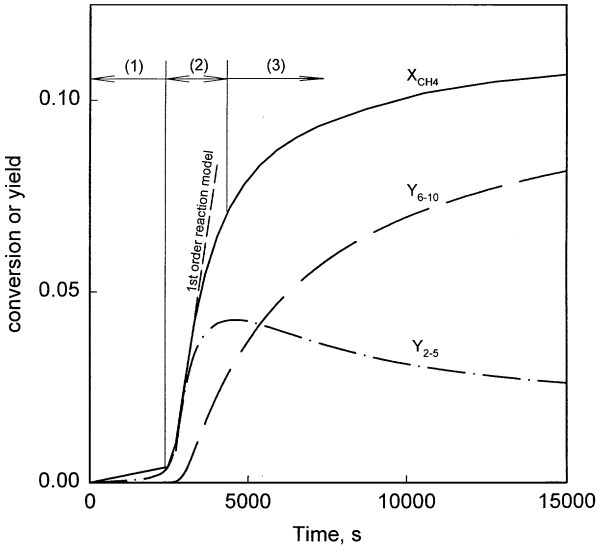

Fig. 2. CH_4 conversion as a function of contact time for homogeneous pyrolysis (1038 K, 0.59 bar).

3. Results and discussion

3.1. Homogeneous methane pyrolysis rate and selectivity in tubular reactors with non-permeable walls

Fig. 1 compares our simulation results using the homogeneous reaction mechanism described in Section 2 with the experimental data of Chen, Back, and Back (1975). This modified Dean model describes these low-conversion experimental data, especially C_2H_2, more accurately than earlier simulations (Dean, 1990). This appears to reflect the availability and incorporation of more accurate thermodynamic data for several of the radicals and the consequent improvement in the estimates of reverse rate constants for all steps involving those radicals.

Fig. 2 shows the predicted methane conversion and the C_2–C_5, C_6–C_{10}, and coke yields at 1038 K and 59 kPa CH_4 at conversions significantly higher than those reported in Fig. 1. The conversion-time trends suggest that methane reaction paths can be divided into three regions. The conversion is very low during an initial period ($t \sim 2400$ s), within which methane reactions are limited by the slow initiation step:

$$CH_4 = CH_3\cdot + H\cdot. \quad (10)$$

The reaction rate then increases at longer times, as a result of the accumulation of $CH_3\cdot$ and $H\cdot$ radicals, which participate in chain transfer reactions; these chain transfer steps form products without the net consumption of free radicals. Finally, the third stage reflects a decrease in methane conversion rate as the reacting mixture approaches equilibrium conversions, which are $\sim$20% at 1038 K. At these low temperatures, however, it takes impractical contact times ($\sim$600 h) to reach even 90% of this equilibrium conversion.

As mentioned above, a pseudo-first-order reaction model is useful in examining the sensitivity of these reactors to the rate of removal of H_2. Since most of the methane conversion occurs in the chain transfer kinetic stage (stage 2), we attempt to describe the methane conversion rates in Fig. 2 using a first-order rate equation:

$$R_{CH_4} = k_{eff} C_{CH_4}. \quad (11)$$

The corresponding comparison between the behavior of this model for a best-fit value of k_{eff} and the detailed simulation results in Fig. 2 led us to conclude that this provides a reasonable representation for the overall behavior of the complete network within the kinetic region where most of the CH_4 conversion takes place. The resulting value of k_{eff} is $7\times10^{-5}\ s^{-1}$ (at 1038 K); it is used to represent *Da* and δ in all subsequent analyses of the sensitivity of the system to changes in reaction or transport parameters. Support for this lumping approach was also obtained by simulating the effect of inlet methane pressure (40–200 kPa) on reaction rates, which led to similar values of k_{eff} at all inlet methane pressures.

3.2. *The effect of* H_2 *on homogeneous methane pyrolysis rate and selectivity*

Before considering the effect of H_2 removal on methane pyrolysis reactions, we examine the influence of added H_2 on homogeneous pyrolysis rate and selectivity. Fig. 3 shows the effects of H_2 on the induction time, t_{in}, the empirical first-order rate constant, k_{eff}, and the equilibrium conversion X_{eq}; these parameters describe the effect of H_2 on the three kinetic stages of homogeneous methane pyrolysis. The equilibrium CH_4 conversion obviously decreases with increasing H_2 concentration, but H_2 also shows a strong kinetic effect. By examining the approach to equilibrium for each elementary step we conclude that steps converting methane to C_2–C_5 attain equilibrium more rapidly than steps that convert C_2–C_5 to C_6–C_{10}. Even in the chain transfer kinetic stage, methane conversion rates, which are characterized by k_{eff}, are influenced by the local equilibration of the steps leading to C_2–C_5. As a result, the presence of H_2 decreases methane pyrolysis rates because it decreases the equilibrium concentration of the required reaction intermediates. Thus, continuous H_2 removal overcomes both

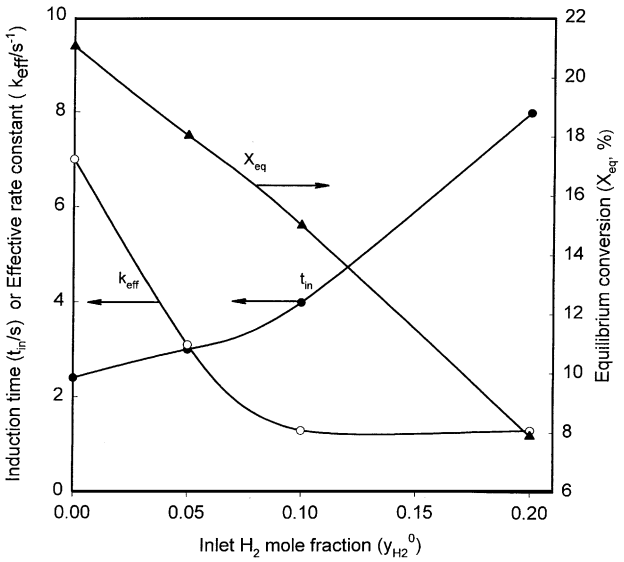

Fig. 3. Effect of H_2 initial partial pressure on induction time, effective rate constant, and equilibrium conversion (1038 K, 0.59 bar).

thermodynamic and kinetic constraints in homogeneous methane pyrolysis pathways.

The effect of H_2 on CH_4 pyrolysis selectivity is much more complex. Figs. 4(a) and (b) show the selectivity to C_2–C_5 and C_6–C_{10} products as a function of CH_4 conversion. At low CH_4 conversions ($X<0.02$), the reacting mixture is far from equilibrium at all inlet H_2 concentration and the selectivity is controlled by the forward rate of each reaction step. At these low conversions, H_2 decreases C_6–C_{10} selectivity and it increases the selectivity to C_2–C_5 products (Fig. 4). H_2 appears to inhibit the formation of C_6–C_{10} products more strongly than the formation of C_2–C_5 products. At higher methane conversions, every elementary step becomes reversible and approaches its corresponding equilibrium; selectivities then become predominately controlled by thermodynamics. At intermediate conversions, reaction steps that form C_2–C_5 products approach equilibrium, but C_2–C_5 products continue to react to form C_6–C_{10} hydrocarbons. As a result, C_2–C_5 selectivities ultimately decrease sharply with increasing contact time. As H_2 concentrations increase, the maximum C_2–C_5 selectivity moves to lower CH_4 conversions. At these intermediate conversions, the selectivity to C_2–C_5 components decreases and the selectivity of C_6–C_{10} components increases with increasing H_2 concentration.

3.3. *The effect of hydrogen removal rate on homogeneous pyrolysis rate and selectivity*

Fig. 5 shows simulation results for methane homogeneous pyrolysis with continuous removal of H_2 along the permeable walls of a tubular reactor. H_2 removal eliminates thermodynamic constraints for the overall

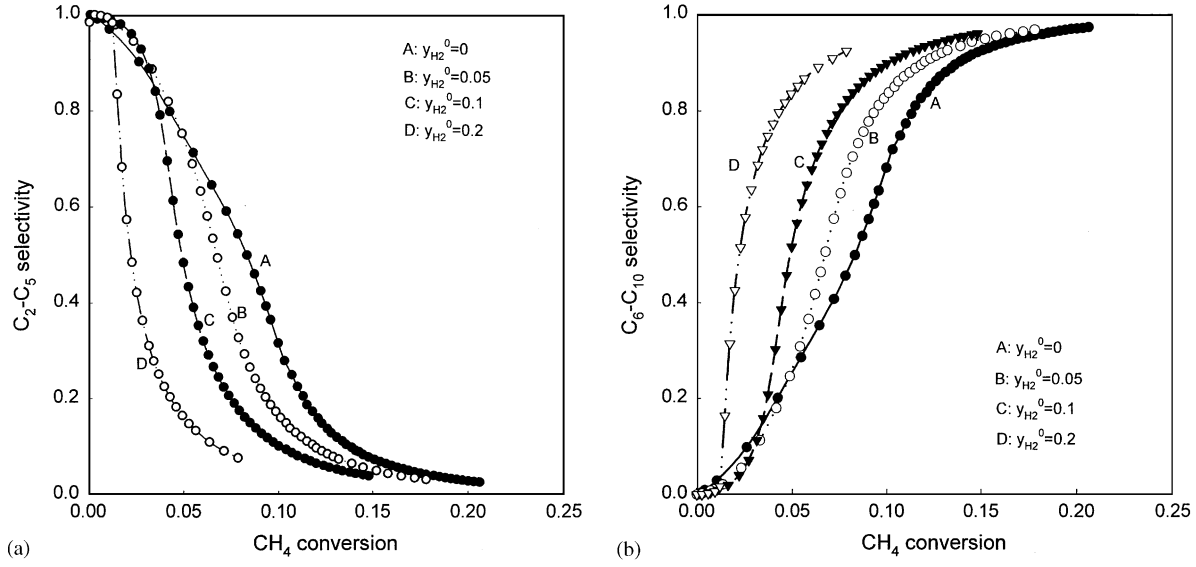

Fig. 4. Effect of hydrogen on homogeneous pyrolysis selectivity (1038 K, 0.59 bar).

pyrolysis reaction; as a result, every elementary step producing hydrogen proceeds only in the forward direction. The removal of H_2, however, does not influence the reaction rate during the critical initial induction period. During this induction period, pyrolysis rates are controlled by slow but irreversible initiation steps, which are far from equilibrium at the low H_2 pressures prevalent during this initial pyrolysis stage. The results shown in Fig. 5 reflect the effects of residence time (as given by the Damkohler number, *Da*) on methane conversion and product yields for a wide range of values for the relative rates of hydrogen formation and removal ($\delta = 10^{-3}$–10^{9}).

For a given contact time (or *Da*), methane conversion increases monotonically as δ increases, because reverse reactions cannot occur in the absence of H_2; complete methane conversions are reached for δ values greater than 1. The residence time (*Da*) required in order to reach a given methane conversion decreases with increasing δ, as a result of an increase in the net forward reaction rate with decreasing H_2 concentration. This is consistent with the simulated effects of H_2 on methane conversion rates discussed in the previous section. These changes occur at values of δ between 0.1 and 10. Values of δ greater than 10 lead to negligible H_2 concentrations at all reactor locations and residence times. Values of δ smaller than 0.1 remove negligible amounts of H_2 and they do not influence local H_2 concentrations throughout the reactor.

At short residence times ($Da \ll 1$), H_2 removal increases C_2–C_5 yields, but these yields decrease at higher contact times (*Da*) because the removal of H_2 also increases the rate at which C_2–C_5 molecules react further to form larger C_{6+} hydrocarbons. These simulations also show that the most abundant pyrolysis products are benzene and naphthalene over the expected range of conversion and contact time. When δ is about 1, C_6–C_{10} yields higher than 90% are predicted. For values of δ between 10 and 10^3, higher H_2 removal rates do not significantly increase C_6–C_{10} yields. Further increases in hydrogen removal rate lead to increasing coke yields at the expense of C_6–C_{10} yields. The simulation results shown in Fig. 5 suggest that H_2 removal can lead to near complete CH_4 conversions with C_6–C_{10} yields greater than 90%, even in the absence of catalytic sites. For purely homogeneous pathways, the required reactor residence times, however, are impractical (>100 h).

The effects of H_2 removal on pyrolysis product yields are shown in Fig. 6 as maximum attainable yields as a function of δ. Maximum C_6–C_{10} yields require intermediate δ values. Small H_2 permeation rates ($\delta < 0.01$) do not remove a significant fraction of the H_2 formed via homogeneous pyrolysis reactions. Very high H_2 permeation rates ($\delta > 10^3$), on the other hand, favor the subsequent conversion of C_6–C_{10} aromatics to polyaromatic hydrocarbons.

Figs. 7(a) and (b) show the effect of H_2 removal rate on the selectivity to C_2–C_5 and C_6–C_{10}, respectively. As H_2 is removed continuously from the reactor, the reaction steps involving hydrogen cannot approach equilibrium, and the selectivity–conversion plots remain in the chain transfer kinetic region at all CH_4 conversion values. As a result, C_2–C_5 selectivities increase and C_6–C_{10} selectivities decrease with increasing H_2 removal rates (δ). The observed decrease in C_6–C_{10} selectivity at high CH_4 conversions reflects the ultimate conversion of C_6–C_{10} products to polyaromatic hydrocarbons and coke.

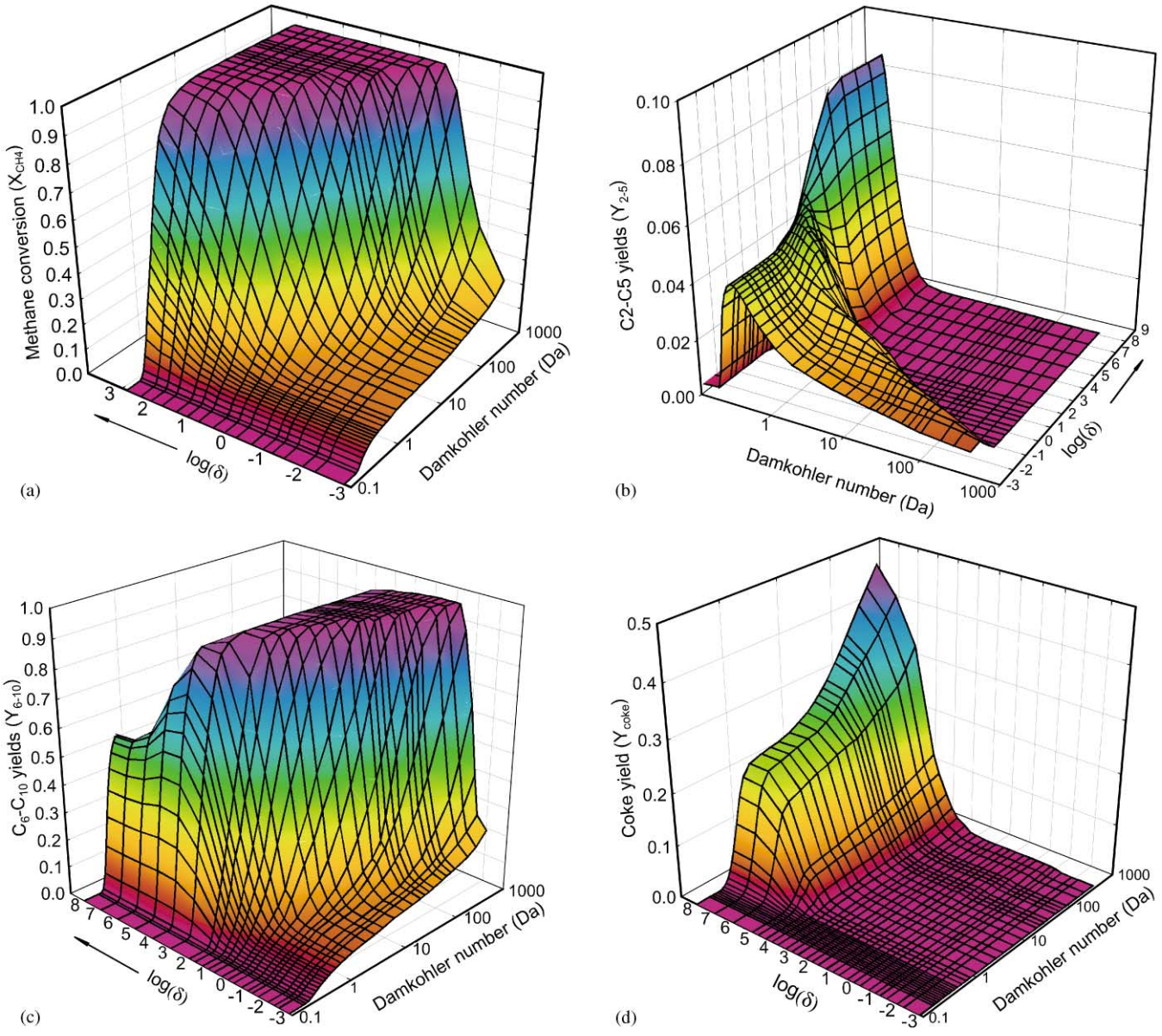

Fig. 5. Effect of hydrogen removal on (a) CH_4 conversion, (b) C_2–C_5 yields, (c) C_6–C_{10} yields, and (d) coke yields (1038 K, 0.59 bar).

The results described above suggest that δ values between 1 and 10 are required in order to attain maximum C_2–C_{10} yields. The defining equation for δ (Eq. (6)) shows that for a given reaction rate, δ depends on the membrane permeability P, the membrane thickness l, and the tube reactor diameter d (proportional to its volume to surface ratio). The membrane permeability is controlled by the nature of the dense or porous ceramic material. For proton-conducting membranes based on $SrCeO_3$ or $SrZrO_3$ perovskites, which appear best suited for methane pyrolysis applications (Schober, Friedrich, & Condon, 1995; Hamakawa et al., 1993; Hamakawa et al., 1994; Borry, Lu, Kim, & Iglesia, 1998), reported hydrogen permeabilities are in the range of 10^{-13}–10^{-12} mol m^{-1} s^{-1} Pa^{-1} at 1000 K. For homogeneous pyrolysis, k_{eff} is 7×10^{-5} s^{-1} at 1038 K. Thus, for a reactor diameter of 1 cm, we estimate the required membrane thickness to be 0.4–4 mm for a δ value of 10. Thus, thick membrane walls provide sufficient hydrogen removal for purely homogeneous pathways, but only because of the very low productivities and large volumes required to achieve significant conversions in these homogeneous reactors. The ultimate requirement for catalytic sites, in the form of radical-generation sites or bifunctional cation-exchanged zeolites (Borry et al., 1998), must lead to $\sim10^3$ increases in reactor productivities in order to reduce the required residence times to practical levels. In such cases, H_2 removal rates must be correspondingly higher and thin membrane films of about 10–100 μm thickness or materials with greater

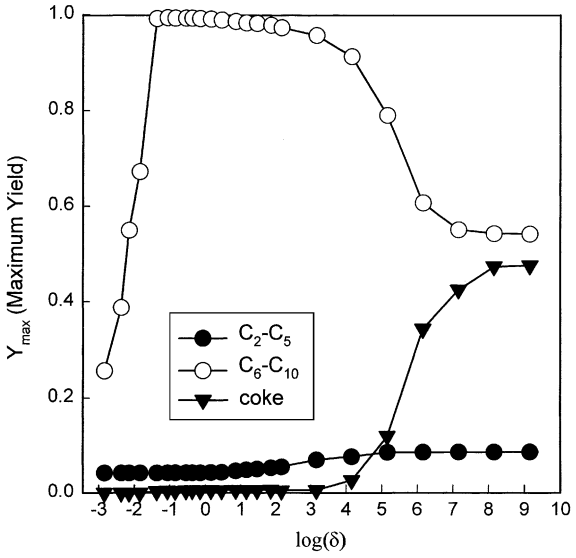

Fig. 6. Effect of hydrogen removal on maximum attainable yields of C_2–C_5, C_6–C_{10} and coke (1038 K, 0.59 bar).

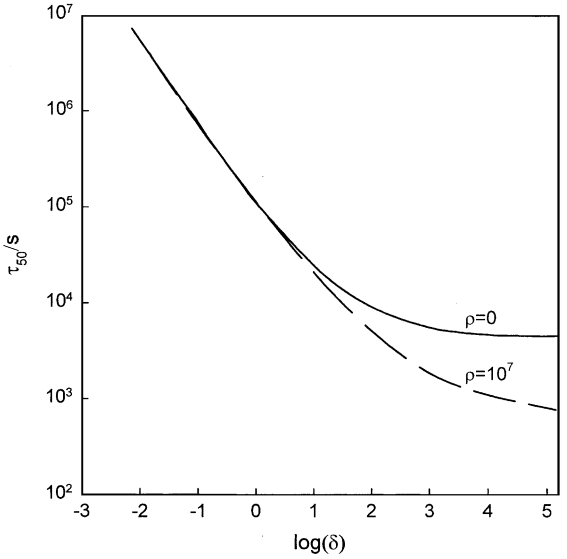

Fig. 8. Required residence time at different hydrogen removal rates (1038 K, 0.59 bar).

permeability will be required for the successful application of membrane reactor concepts in CH_4 conversion (Lu & Iglesia, 1999; Borry et al., 1998).

The solid line in Fig. 8 shows the residence time required to attain 50% conversion, τ_{50}, for purely homogeneous membrane reactors. H_2 removal decreases τ_{50} significantly for values of δ between 10^{-3} and 10^3. Higher δ values show much weaker effects on τ_{50}. Even at δ values above 10, the residence times required are greater than 1 h and they remain impractical for industrial practice. The removal of H_2, however, eliminates all thermodynamic constraints. The kinetic enhancement provided by H_2 removal is not sufficient to make purely homogeneous pyrolysis process practical and this accounts for the disappointing results obtained in previous experimental efforts. It is not feasible to increase methane pyrolysis rate solely by raising the reaction temperature, because higher temperatures lead to the predominant formation of polynuclear aromatics and coke. Also, higher temperatures (>1100 K) cause perovskite materials to conduct also oxygen anions, which lead to the formation of undesired CO_x products in the methane side of the membrane reactor. Thus, it appears from these simulation results that a catalytic material will be required for practical applications of membrane reactors. In the next section, we describe the effects of catalytic sites that

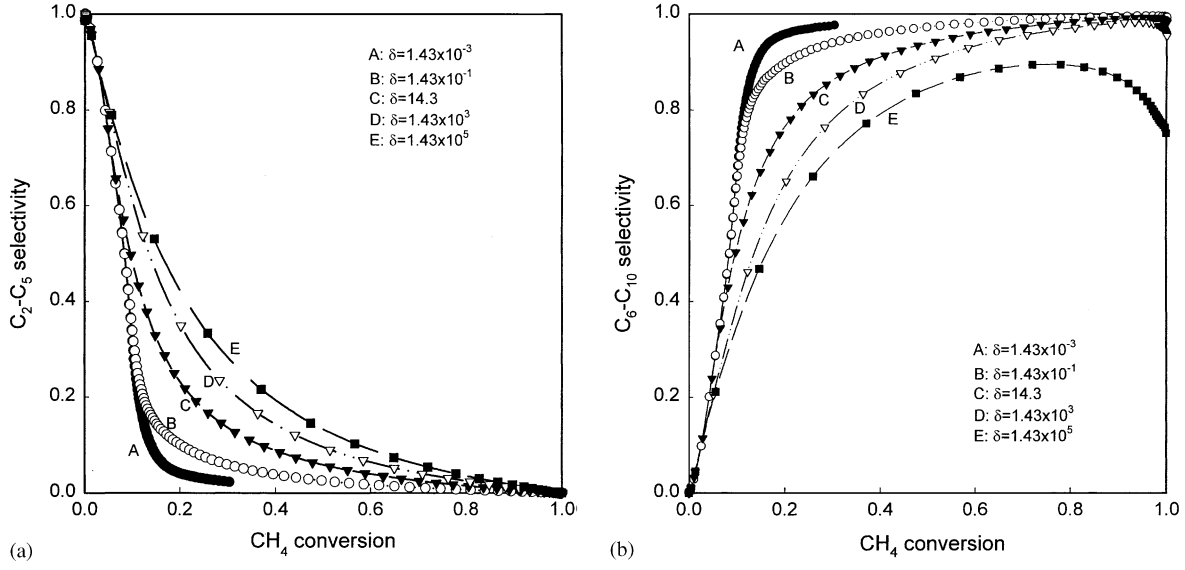

Fig. 7. Effect of hydrogen removal on C_2–C_5 and C_6–C_{10} selectivities (1038 K, 0.59 bar).

merely increase the rate of methyl radical generation during the induction period. In a later report, we describe the behavior of a more complex catalytic system consisting of bifunctional materials with ethylene formation and conversion sites.

3.4. Effect of catalytic sites for the formation of methyl radicals from methane

In the absence of a catalyst that can limit chain growth via steric effects or shape selectivity, pyrolysis reactions must be carried out at low temperatures in order to limit the rate of formation of undesired C_{11+} hydrocarbon. The residence times required for significant CH_4 conversions via exclusively homogeneous pathways are impractical, even with rapid H_2 removal, which increases reaction rates, decreases required residence times, and eliminates thermodynamic constraints.

According to the simulation results shown in Fig. 5, the Damkohler number, *Da*, must be greater than 20 in order to attain high C_6–C_{10} yields. The first-order reaction rate constant for homogeneous pyrolysis of methane is $7 \times 10^{-5}\ s^{-1}$, and the required reactor residence time is $\sim$100 h. At 1038 K for pure methane reactants, the initiation step (10)

$$CH_4 \overset{k_1}{=} CH_3\cdot + H\cdot$$

is very slow ($k_1 = 2.21 \times 10^{-7}\ s^{-1}$) (Dean, 1990) and limits overall reaction rates. Catalytic sites that can activate C–H bonds in CH_4 to form methyl and hydrogen radicals may be able to increase overall pyrolysis rate. Here, we examine the effect of catalytic activation of methane by introducing a catalytic surrogate for the elementary step shown in Eq. (1) into the homogeneous kinetic network. We consider only the effects of faster methyl radical formation step on methane pyrolysis rates by introducing a hypothetical catalytic surface capable of dissociation of methane to form methyl radicals, as experimentally demonstrated in oxidative coupling reactions.

The effects of methane activation sites on CH_4 conversion and product yields are shown in Figs. 9 and 10, respectively. In these figures, the parameter $\rho = k_{s1}/k_1$, represents the relative magnitude of the catalytic rate constant (k_{s1}) and the rate constant for the purely homogeneous activation of methane (k_1). The rate constant of methane catalytic dissociation reaction, k_{s1}, can be estimated from the surface area, the density of active sites, site turnover rate and particle density of typical catalysts. Values of ρ as high as 10^8 are readily attainable (Reyes, Iglesia, & Kelkar, 1993). Catalytic sites shorten and ultimately eliminate the induction period (Fig. 9). Therefore, sites that merely form methyl radicals, which then enter homogeneous methane pyrolysis pathways, can decrease

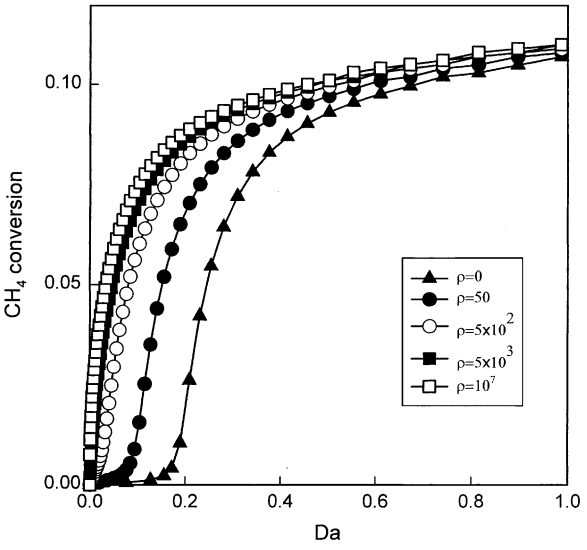

Fig. 9. Effect of catalytic CH_4 activation sites on CH_4 conversion (1038 K, 0.59 bar).

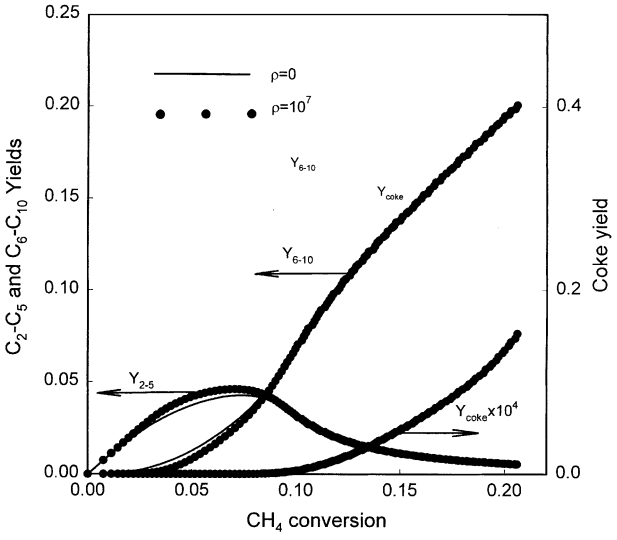

Fig. 10. Effect of CH_4 catalytic activation site on product yields (1038 K, 0.59 bar).

markedly the residence time required to reach practical methane conversions (Fig. 9). Such sites, however, do not influence the yields and selectivities characteristic of homogeneous pathways (Fig. 10). The selectivity–conversion trends remained unchanged by catalytic initiation steps, but a given CH_4 conversion level can be reached at a much shorter residence time, primarily as a result of a much shorter induction period.

The predominant CH_4 pyrolysis products are ethylene, benzene, and naphthalene at 823–1073 K. Thus, we may refer to their inter-conversion using the non-elementary steps below in order to discuss the behavior of the overall reaction, even when the simulations rigorously

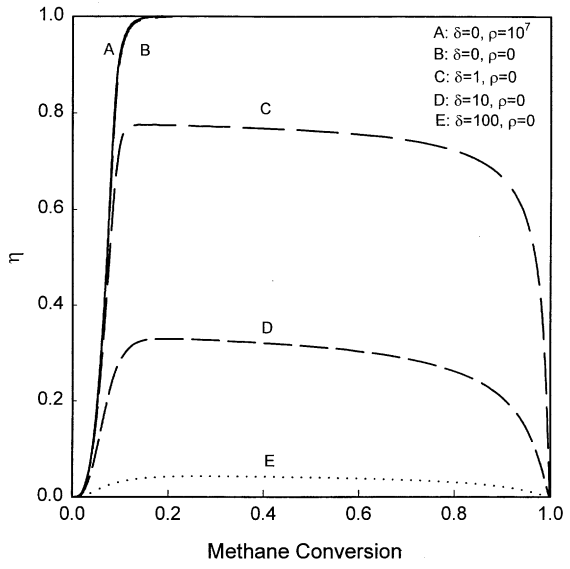

Fig. 11. Approach to equilibrium for the methane to ethylene reaction (1038 K, 0.59 bar).

include the detailed steps included in the homogeneous–heterogeneous kinetic network:

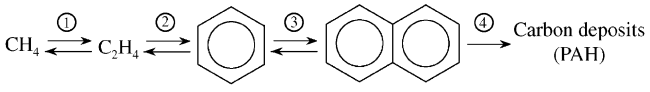

Surface-catalyzed CH_4 activation steps increase reaction rates at low conversions. At higher conversions, surface-initiated and purely homogeneous pathways lead to similar rates, because the reaction products also "catalyze" homogeneous reaction rates via chain transfer steps that abstract hydrogen atoms from methane reactant. Therefore, reaction rate and product selectivities depend only weakly on the rate of initial methane activation steps, because step 1 approaches its unfavorable equilibrium as H_2 is formed in subsequent dehydrogenation steps ($2CH_4 = C_2H_4 + 2H_2$ is limited to $\sim 8\%$ conversion at 1038 K). The approach to equilibrium for step 1 can be calculated as

$$\eta = \frac{[C_2H_4][H_2]^2}{[CH_4]^2}\frac{1}{K_{EQ,1}},$$

where η is equal to 0 for an irreversible reaction and it equals 1 at equilibrium. Then the net rate of reaction becomes $k_{f1}[CH_4](1-\eta)$. From lines A and B in Fig. 11 we observe that without removal of H_2 ($\delta = 0$) catalytic activation of methane has no influence on η at a given conversion. At methane conversions of 10%, the value of η is 93%; therefore, the net forward rate of methane conversion reaction and the product distribution are determined only by the rate of the subsequent C_2H_4 conversion to products (via steps 2–4). Catalytic sites that activate only CH_4 increase initial methane conversion rates but cannot achieve higher conversions ($>10\%$) at practical reactor residence times because of thermodynamic limitations for the methane to ethylene conversion reaction.

In order to increase the rate of the overall methane conversion reaction, equilibrium limitations must be overcome by catalyzing C_2H_4 conversion pathways and/or by removing one of the products of reaction (H_2 or C_2H_4). Fig. 11 also shows η values at different values of hydrogen removal rate. By removing hydrogen from the reactor, η can be decreased markedly; as a result, the net forward rate of methane conversion increases. Fig. 8 shows the effect of hydrogen removal rates on the residence time required to attain 50% conversion (τ_{50}) in homogeneous ($\rho = 0$) and homogeneous–heterogeneous reactors ($\rho = 10^7$). H_2 removal decreases τ_{50} in homogeneous–heterogeneous reactors for values of δ greater than 1 by removing thermodynamic limitations on the concentration of C_2 hydrocarbons available for further conversion to C_6–C_{10} aromatics. Reactions rates become limited by the subsequent conversion of C_2 hydrocarbons to C_6–C_{10} products, which are unaffected by surface catalysis because the catalytic sites activate only CH_4. Catalytic sites that activate C–H bonds in CH_4 can also activate the weaker C–H bonds in ethane, and thus remove the remaining kinetic barriers preventing conversion of CH_4 at practical reactor residence times. We will address in a subsequent study the detailed simulations for Mo/H-ZSM5 catalysts, which increase the rate of the subsequent oligomerization and cyclization using acid sites contained within shape-selective environment.

A marked effect of methane activation sites is observed for ρ values between 1 and 10^3 (Fig. 9). Higher ρ values do not influence methane conversion rate or selectivity. The pseudo-first-order reaction rate (k_{eff}) of homogeneous methane pyrolysis is $7 \times 10^{-5}\,s^{-1}$ at 1038 K; it reflects the characteristic reaction time in the fast reaction region (chain transfer region). When ρ is 10^3, the ratio of k_{s1}/k_{eff} is about 1, which means that for ρ that greater than 10^3, the initial methane activation is no longer the rate-determining step. Increasing methane conversion rates in this fast reaction region requires that we influence the new rate-determining steps. It is likely that the slow conversion of an equilibrated mixture of C_2–C_5 hydrocarbons to more stable aromatics leads to quasi-equilibrated concentrations of ethane and ethene. Here, the role of a catalyst, such as Mo/H-ZSM5, that is able to catalyze the conversion of alkanes to aromatics via bifunctional pathways, would remove such kinetic barriers. Neither purely homogeneous pathways nor selective catalytic formation of CH_3 radical can influence the rate of these reactions of higher alkanes and thus the overall rate of CH_4 reactions.

We have also explored the possible influence of ethane on homogeneous methane pyrolysis rates. The reaction rate of ethane to form methyl radical is 10^4 times greater

than that of methane, so the introduction of ethane in the feed could lead to a marked increase in methyl radical concentrations and to higher methane pyrolysis rates. Our simulations show, however, that the presence of ethane in the feed does not influence methane conversion rates. In fact, methane remains essentially unconverted until most ethane molecules were converted. The approach to equilibrium parameters for each elementary step, η_i, showed that the high methyl radical concentrations prevalent during ethane conversion cause all elementary steps involving methane to proceed in the direction of methane formation or to approach equilibrium. Therefore, the addition of ethane in the system actually inhibits the net rate of conversion of methane.

5. Conclusions

Non-oxidative CH_4 pyrolysis with hydrogen removal was simulated using detailed reaction-transport model and available literature data and correlations. The presence of hydrogen in the reaction medium strongly influences methane conversion and selectivity through both thermodynamic and kinetic effects. The equilibrium conversion and the initial reaction rate of methane decrease with increasing hydrogen partial pressure. By removing hydrogen, thermodynamic constraints are completely removed. It is then possible to attain nearly 100% conversion of methane with $C_{2\text{-}10}$ yields greater than 90%, but it is impractical to attain high $C_{2\text{-}10}$ yields via homogeneous pathways because of the long required residence times. The introduction of catalytic sites capable of initiating pyrolysis by forming methyl and hydrogen radicals increases CH_4 conversion rates at low methane conversions, but they do not influence the maximum attainable C_2–C_{10} yields because at high methane conversions, the net forward rate of methane pyrolysis is controlled mainly by the conversion of C_2 to higher molecular weight hydrocarbons.

Notation

d inner diameter of reactor, m
Da Damkohler number
f_i dimensionless rate expression for reaction i
F_{j_0} mole feed flow rate of component j, mol m^{-2} s^{-1}
k_{eff} empirical pseudo-first-order rate constant of CH_4 conversion, s^{-1} or cm^3 mol^{-1} s^{-1}
k_f forward reaction rate constant, s^{-1} or cm^3 mol^{-1} s^{-1}
k_i rate constant of reaction i, mol m^{-3} s^{-1}
k_r reverse reaction rate constant, s^{-1} or cm^3 mol^{-1} s^{-1}
k_{s1} CH_4 catalytic activation rate constant, s^{-1}
$\boldsymbol{K}$ equilibrium constant vector
l membrane thickness, m
L reactor length, m
$\boldsymbol{p}$ partial pressure vector, Pa
P permeability of hydrogen through membrane, mol m^{-1} Pa^{-1} s^{-1}
P_f permeability of fast component, mol m^{-1}Pa^{-1} s^{-1}
P_T total pressure, Pa
q_j dimensionless flow rate of component j in permeate side, mole flow rate/mole feed flow rate
$\boldsymbol{R}_j$ formation rate of component j, mol m^{-3} s^{-1}
t_{in} induction time, s
X_{eff} equilibrium conversion
y_{jt} mole fraction of component j on tube side
y_{js} mole fraction of component j on shell side

Greek letters

α permeability ratio, defined by Eq. (8)
β reaction rate constant ratio, defined by Eq. (9)
δ ratio of permeation rate to reaction rate, defined by Eq. (7)
η approach to equilibrium parameter, defined by Eq. (20)
λ_{ij} stoichiometric coefficient for species j in reaction i
ρ rate constant ratio for catalytic and homogeneous activation of CH_4
τ_{50} residence time required to attain 50% conversion, s
ϕ_j dimensionless flow rate of component j in reaction side, mole flow rate/mole feed flow rate

Acknowledgements

This work was supported by the Division of Fossil Energy of the United States Department of Energy (Contract DE-AC03-76SF00098) under the technical supervision of Dr. Daniel Driscoll. The authors gratefully acknowledge Dr. Anthony M. Dean and Dr. Sebastian C. Reyes of the Corporate Research Labs of Exxon Research and Engineering Company and Prof. Michael Frenklach of the University of California at Berkeley for their help with the homogeneous kinetic model and with the thermodynamic data used in these simulations.

References

Andersen, A., Dahl, I. M., Jens, K.-J., Rytter, E., & Slagtern, A. (1989). Hydrogen acceptor and membrane concepts for direct methane conversion. *Catalysis Today*, *4*, 389–397.

Benson, S. W. (1976). *Thermochemical kinetics: Methods for the estimation of thermochemical data and rate parameters* (2nd ed.). New York: Wiley.

Borry, R. W., Lu, E. C., Kim, Y. H., & Iglesia, E. (1998). Non-oxidative catalytic conversion of methane with continuous hydrogen removal. In A. Parmaliana et al. (Eds.), *Studies in surface science and catalysis*, Vol. 119 (pp. 403–410). Amsterdam: Elsevier.

Chen, C.-J., Back, M. H., & Back, R. A. (1975). The thermal decomposition of methane. I. Kinetics of the primary decomposition to $C_2H_6 + H_2$; rate constant for the homogeneous unimolecular dissociation of methane and its pressure dependence. *Canadian Journal of Chemistry*, *53*, 3580.

Dean, A. M. (1990). Detailed kinetic modeling of autocatalysis in methane pyrolysis. *Journal of Physical Chemistry*, *94*, 1432–1439.

Gueret, C., Daroux, M., & Billaud, F. (1997). Methane pyrolysis: Thermodynamics. *Chemical Engineering Science*, *52*(5), 815–827.

Hamakawa, S., Hibino, T., & Iwahara, H. (1993). Electrochemical methane coupling using protonic conductors. *Journal of the Electrochemical Society*, *140*(2), 459.

Hamakawa, S., Hibino, T., & Iwahara, H. (1994). Electrochemical hydrogen permeation in a proton-hole mixed conductor and its application to a membrane reactor. *Journal of the Electrochemical Society*, *141*(7), 1720–1725.

Hsieh, H. P. (1996). *Inorganic membranes for separation and reaction*. Amsterdam: Elsevier.

Ito, T., & Lunsford, J. H. (1985). Synthesis of ethylene and ethane by partial oxidation of methane over lithium-doped magnesium oxide. *Nature*, *314*, 721–722.

Jiang, Y., Yentekakis, I. V., & Vayenas, C. G. (1994). Methane to ethylene with 85 percent yield in a gas recycle electrocatalytic reactor-separator. *Science*, *264*, 1563–1566.

Karni, M., Oref, I., & Burcat, A. (1991). Ab-initio calculations and ideal gas thermodynamic functions of cyclopentadiene and cyclopentadiene derivatives. *Journal of Physical Chemistry Reference Data*, *20*(4), 665–683.

Kee, R. J., & Lutz, A. (1991). *Interactive driver for STANJAN-III equilibrium program*. Sandia National Laboratories, Livermore, CA 94550.

Kee, R. J., Rupley, F. M., & Miller, J. A. (1990). *CHEMKIN-II: A FORTRAN chemical kinetics package for the analysis of gas-phase chemical kinetics*. Sandia Report SAND89-8009, UC-401, Sandia, NM.

Keller, G. E., & Bhasin, M. M. (1982). Synthesis of ethylene via oxidative coupling of methane. I. Determination of active catalysts. *Journal of Catalysis*, *73*, 9–19.

Langguth, J., Dittmeyer, R., Hofmann, H., & Tomandl, G. (1997). Studies on oxidative coupling of methane using high-temperature proton-conducting membranes. *Applied Catalysis A: General*, *158*, 287–305.

Lay, T. H., Bozzelli, J. W., Dean, A. M., & Ritter, E. R. (1995). Hydrogen atom bond increments for calculation of thermodynamic properties of hydrocarbon radical species. *Journal of Physical Chemistry*, *99*, 14514–14527.

Lu, E. C., & Iglesia, E. (1999). Synthesis of yttria-doped strontium-zirconium oxide powders via ammonium glycolate combustion methods as precursors for dense ceramic membranes. *Journal of Materials Science*, submitted for publication.

Lunsford, J. H., Rosynek, M. P., Wang, D. (1995). *Proceedings of the fourth international natural gas symposium*, Kruger National Park, South Africa.

Reyes, S. C., Iglesia, E., & Kelkar, P. (1993). Kinetic-transport models of bimodal reaction sequences — I. Homogeneous and heterogeneous pathways in oxidative coupling of methane. *Chemical Engineering Science*, *48*, 2643–2661.

Ritter, E. R., & Bozzelli, J. W. (1991). THERM: Thermodynamic property estimation for gas phase radicals and molecules. *International Journal of Chemical Kinetics*, *23*, 767–778.

Rokstad, O. A., Olsvik, O., Jessen, B., & Holmen, A. (1992). Ethylene, acetylene and benzene from methane. In: L. F. Albright, B. L. Cynes, S. Novak (Eds.), *Novel production methods for ethylene, light hydrogens and aromatics* (pp. 259–273). New York: Marcel Dekker.

Schober, T., Friedrich, J., & Condon, J. B. (1995). Effective hydrogen diffusivity in $SrCe_{0.95}Yb_{0.05}O_{3-\alpha}$ and $SrZr_{0.95}Y_{0.05}O_{3-\alpha}$. *Solid State Ionics*, *77*, 175–179.

Solymosi, F., Cserenyi, J., Szoke, A., Bansagi, T., & Oszko, A. (1997). Aromatization of methane over supported and unsupported Mo-based catalysts. *Journal of Catalysis*, *165*, 150–161.

Solymosi, F., Erdohelyi, A., & Szoke, A. (1995). Dehydrogenation of methane on supported molybdenum oxides. Formation of benzene from methane. *Catalysis Letters*, *32*, 43–54.

Stull, D. R., Edgar, F., Westrum, J., & Sinke, G. C. (1987). *The chemical thermodynamics of organic compounds* (p. 865). Malabar: Robert E. Krieger Publishing Co.,

Tonkovich, A. L., Carr, R. W., & Aris, R. (1993). Enhanced C_2 yields from methane oxidative coupling by means of a separative chemical reactor. *Science*, *262*, 221–223.

Tsotsis, T. T., Champagnie, A. M., Vasileiadis, S. P., & Liu, P. K. T. (1993). Catalytic membrane reactors. In E. R. Becker, & C. J. Pereira (Eds.), *Computer-Aided Design of Catalysts (pp. 471–551)*. New York: Marcel Dekker.

Wnag, H., & Frenklach, M. (1997). Detailed kinetic modeling study of aromatics formation in laminar premixed acetylene and ethylene flames. *Combustion and Flame, 111,* 173–221.

Wang, D., Lunsford, J. H., & Rosynek, M. P. (1996). Catalytic conversion of methane to benzene over Mo/ZSM-5. *Topics in Catalysis*, *3*, 289–297.

Wang, L., Tao, L., Xie, M., & Xu, G. (1993). Dehydrogenation and aromatization of methane under non-ozidizing conditions. *Catalysis Letters*, *21*, 35–41.

Woldman, L. S., & Sokolovskii, V. D. (1991). Electrocatalytic methane coupling in the abscence of oxygen on a high-temperature proton-conducting electrolyte. *Catalysis Letters*, *8*, 61–66.